electronics

MDPI

Article

Toward an Advanced Human Monitoring System Based on a Smart Body Area Network for Industry Use

Kento Takabayashi [1,*], Hirokazu Tanaka [2] and Katsumi Sakakibara [1]

[1] Department of Information and Communication Engineering, Faculty of Computer Science and Systems Engineering, Okayama Prefectural University, Okayama 719-1197, Japan; sakaki@c.oka-pu.ac.jp
[2] Graduate School of Information Sciences, Hiroshima City University, 3-4-1 Ozuka-Higashi, Asa-Minami-Ku, Hiroshima 731-3194, Japan; hi.tanaka@m.ieice.org
* Correspondence: takabayashi.kento.xp@gmail.com; Tel.: +81-866-94-2104

Abstract: This research provides a study on a smart body area network (SmartBAN) physical layer (PHY), as an of the Internet of medical things (IoMT) technology, for an advanced human monitoring system in industrial use. The SmartBAN provides a new PHY and a medium access control (MAC) layer, improving its performance and providing very low-latency emergency information transmission with low energy consumption compared with other wireless body area network (WBAN) standards. On the other hand, IoMT applications are expected to become more advanced with smarter wearable devices, such as augmented reality-based human monitoring and work support in a factory. Therefore, it is possible to develop more advanced human monitoring systems for industrial use by combining the SmartBAN with multimedia devices. However, the SmartBAN PHY is not designed to transmit multimedia information such as audio and video. To address this issue, multilevel phase shift keying (PSK) modulation is applied to the SmartBAN PHY, and the symbol rate is improved by setting the roll-off rate appropriately to realize the system. The numerical results show that a sufficient link budget, receiver sensitivity and fade margin were obtained even when those approaches were applied to the SmartBAN PHY. The results indicate that these techniques are required for high-quality audio or video transmission, as well as vital sign data transmission, in a SmartBAN.

Keywords: Internet of Medical Things; SmartBAN; human monitoring system; industry use case; cross-layer design

Citation: Takabayashi, K.; Tanaka, H.; Sakakibara, K. Toward an Advanced Human Monitoring System Based on a Smart Body Area Network for Industry Use. *Electronics* **2021**, *10*, 688. https://doi.org/10.3390/ electronics10060688

Academic Editor: Bersain A. Reyes, Jo Woon Chong and Oh Seok Kwon

Received: 14 February 2021
Accepted: 11 March 2021
Published: 15 March 2021

1. Introduction

Due to the evolution of technology and platforms, such as sensing, mobile computing and cloud servers, the Internet of things (IoT) is recognized as very important technology worldwide. Applications using IoT technology are widely deployed. In particular, the Internet of medical things (IoMT) is attracting attention for constructing home medical care and telemedicine systems using medical and healthcare devices and robots [1,2]. The system involves wearable, wireless vital sign sensors or medical robots. One type of technology supporting the development of the IoMT system is the wireless body area network (WBAN), which flexibly connects biosensors placed near the surface of the body [3–10]. WBANs consist of a collection of low-power, miniaturized, invasive or noninvasive lightweight sensors with wireless communication capabilities that operate near the human body. Numerous studies have been conducted on human vital information monitoring systems using WBANs. For example, sensor nodes for measuring blood oxygen saturation and heart rate, designed based on the near-infrared dynamic spectrum method for WBANs, were proposed in [11]. The authors of [12] designed a prototype to facilitate reliable fall detection and to classify several fall types and human activities. In [13], a trust-based communication scheme to ensure the reliability and privacy of WBANs was proposed for remote patient monitoring.

Furthermore, system specifications for a physical layer (PHY) and a medium access control layer (MAC) in smart body area networks (SmartBANs) were issued in April 2015 [14–16]. These specifications represent a standard for medical care and other forms of health care advanced by the European Telecommunications Standards Institute (ETSI). Compared with a main WBAN standard, such as IEEE Std. 802.15.6, a SmartBAN provides new PHY layer and MAC layer functionalities, which improve its performance and provide very low-latency emergency messaging with low energy consumption [14–17]. Several health monitoring systems using SmartBAN have also been studied [18,19]. The authors of [18] designed a blood pressure fluctuation estimation monitoring system utilizing a SmartBAN. Discussion has also been held on the feasibility of smart cities using biometric information collected through the SmartBAN in [19].

On the other hand, IoMT applications are expected to become more advanced with smarter wearable devices [20,21]. For example, augmented reality (AR) smart glasses have become increasingly popular and been identified as an important technology for supporting operators in smart factories [22]. Research has designed and developed a framework for the support of remote maintenance based on AR by creating suitable communication channels between shop floor technicians and expert engineers, utilizing real-time feedback from the operator's field of view [23]. The authors of [24] also developed a cloud-based, service-oriented system that implemented AR technology for remote maintenance by enabling cooperation between the on-the-spot technician and the manufacturer with smart glasses. By using smart glasses, a worker in a factory can obtain more detailed information from an operator, while an operator can monitor the behavior recognition of a worker by visual and auditory information from smart glasses [25]. Therefore, it is possible to develop more advanced human monitoring systems for industrial use by combining a SmartBAN with multimedia devices such as smart glasses. Related research to realize such a system was introduced as follows: The authors of [26] proposed an innovative and flexible enhanced throughput and reduced overhead (FETRO) MAC protocol for the SmartBAN. In [26], the sensor node data rate requirements were considered while assigning the scheduled access slot duration. Another work presented a SmartBAN PHY and MAC configuration framework that lengthened the sensor battery lifespan through reducing the transceivers' consumed energy [27]. In particular, a link adaptation scheme considering channel quality was combined with a resource allocation algorithm that derived the duration of the interbeacon intervals and transmission periods of sensors [27]. However, those studies did not consider the improvement of the PHY throughput. In other words, more network throughput than that of the current SmartBAN PHY cannot be achieved. Furthermore, the SmartBAN PHY is not designed to transmit multimedia information such as audio and video [14–16]. Specifically, it is not possible to satisfy these desired data rates and latencies when transmitting high-quality audio or video data, since the maximum data rate of the SmartBAN PHY can only reach 1 Mbit per second. Thus, it is necessary to improve the SmartBAN PHY to enable streaming transmission of this type of information.

To address this issue, this research investigates the following approaches for the purpose of improving the data rate of the SmartBAN PHY. The first one is applying multilevel phase shift keying (PSK) modulation, and the second one is increasing the symbol rate. These approaches do not significantly change the specifications of the SmartBAN. In addition, these methods are also expected to improve the data rate while suppressing the energy consumption because their implementation is not complicated. It is confirmed that a sufficient link budget, receiver sensitivity and fade margin can be obtained even when those methods are applied from the numerical results obtained by the mathematical model and computer simulation assuming several channel conditions. In addition, the numerical results show that those types of technology are necessary for high-quality audio or video transmission in the SmartBAN. The study on whether the SmartBAN can be used for industrial use is novel because it has not been considered in previous studies. In addition, this research contributes to the fact that SmartBAN can be effectively used not only for medical and healthcare applications but also for other applications by amending the PHY.

The remainder of this paper is organized as follows. In Section 2, the SmartBAN PHY and MAC layers are summarized. In Section 3, the system model proposed in the research is introduced. The numerical results of the performance evaluation are provided in Section 4. Conclusions and suggestions for future research are presented in Section 5.

2. SmartBAN Specifications

2.1. Physical Layer

2.1.1. Frequency Band

The SmartBAN PHY consisted of two different types of logical channels operating in the 2.4 GHz unlicensed industrial, scientific and medical (ISM) frequency band. These were the control channel (CCH) and the data channel (DCH). The CCH is utilized only for broadcasting a CCH beacon (C-Beacon) by the hub. On the other hand, bidirectional sensor data and control and management information data between the hub and the nodes are transmitted using the DCH.

The utilized spectrum was divided into 40 channels, each having a 2 MHz bandwidth. The 40 center frequencies were equally distributed between 2.402 GHz and 2.480 GHz. Three channels, with channel numbers 1, 12 and 39, were assigned for the CCH, and the other 37 channels were reserved for the DCH. One CCH and one DCH were utilized within one SmartBAN, and those were selected by the hub. Different DCHs were used by neighboring SmartBANs for coexistence management. Unlike Bluetooth Low Energy (BLE), channel hopping is not supported in SmartBAN PHY.

2.1.2. Packet Format, Modulation and Coding Scheme

Figure 1 presents the packet format in the physical layer. The physical layer protocol data unit (PPDU) had a two-octet preamble—1010101010101010—used for frequency synchronization, timing synchronization and automatic gain control. The physical layer convergence protocol (PLCP) header consisted of the packet length, the PHY scheme and other components. It was encoded by the (36, 22) shortened BCH code as an error-correcting code (ECC) and CRC-4-ITU as an error-detecting code. The physical layer service data unit (PSDU) was either an encoded or uncoded MAC protocol data unit (MPDU). The MPDU was encoded by CRC-8 (-CCITT) and CRC-16 (-CCITT) as an error-detecting code.

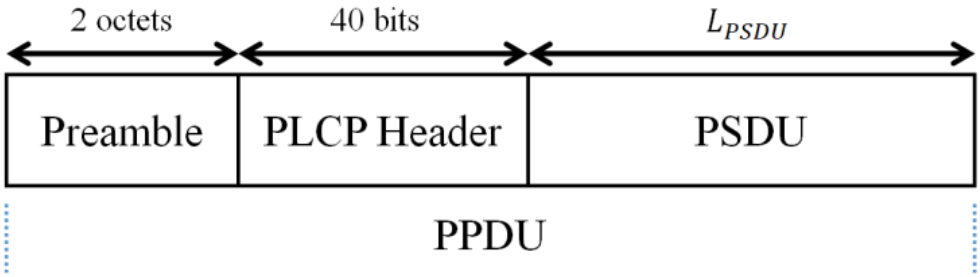

Figure 1. Packet format at the physical layer (PHY).

In the SmartBAN PHY, Gaussian frequency shift keying (GSFK) with a bandwidth-bit period product BT = 0.5 and modulation index h = 0.5 was utilized as a modulation scheme. However, as an error-control scheme in the SmartBAN PHY, a scheme of repeatedly transmitting PPDUs and a scheme encoding the MPDU by using the (127, 113) BCH code as an ECC may be used. In the method of repeated transmission, it is possible to set the number of repetitions N_R = 2, 4. For (127, 113) BCH encoding, the following generator polynomial is used:

$$g(x) = x^{14} + x^9 + x^8 + x^6 + x^5 + x^4 + x^2 + x + 1 \quad (1)$$

Then, the (36, 22) shortened BCH code used in the PLCP header is generated based on the (127, 113) BCH code. It is also possible to use these schemes in combination. Table 1 summarizes the throughput in the PHY.

Table 1. PHY throughput.

Symbol Rate R_s (Mega-Symbol/sec, Msps)	Coding Rate	N_R	Data Rate (Mbit/sec)
1.0	1	1	1.0
1.0	1	2	0.5
1.0	1	4	0.25
1.0	113/127	1	0.89
1.0	113/127	2	0.44
1.0	113/127	4	0.22

2.2. Medium Access Control Layer

The SmartBAN superframe, called the interbeacon interval (IBI), was divided into three channel access periods, as shown in Figure 2: the scheduled access period (SAP), the control and management (C/M) period and the inactive period. SmartBAN provides three different mechanisms. The SAP was used only for data frame transmission and utilizes time division multiple access (TDMA). On the other hand, the C/M period was basically introduced for control and management information between the nodes and the hub, and it utilized slotted ALOHA channel access. The C/M period was available for all the nodes that were ready to transmit the data frame. A node started as a slotted ALOHA channel access session by transmitting in the C/M period with a contention probability (CP) determined by the user priorities defined in Table 2. The range of CPs for different user priority levels is listed in Table 3. At the beginning of each time slot in the C/M period, a node chose its CP as follows:

1. The user priority of its traffic was determined according to Table 2;
2. The range of its CP based on the user priority of its traffic was obtained according to Table 3;
3. If the node had successfully completed or had not begun a slotted ALOHA channel access session previously, its CP was set to $CP_{\max}$;
4. If the node did not successfully complete a slotted ALOHA channel access session in the last attempt:
   - If it had failed m times consecutively, where m is an odd number, it kept its unchanged CP;
   - In the event that it had failed n times consecutively, where n is an even number, it halved its CP if the CP was greater than or equal to $2 \times CP_{\min}$ or kept its CP unchanged otherwise.

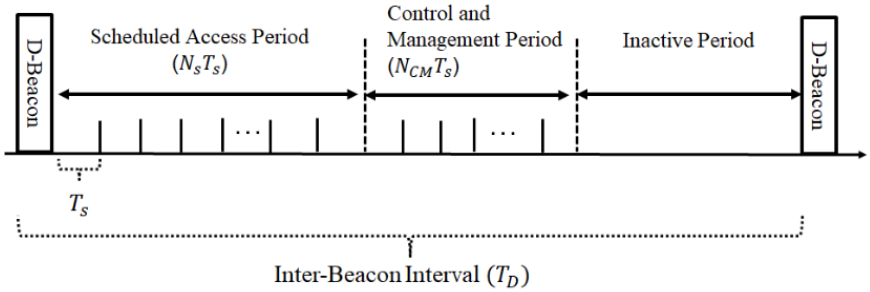

Figure 2. Access periods in the data channel (DCH).

Table 2. List of user priorities.

User Priority	Data Type
0	Low Priority
1	Mid Priority
2	High Priority
3	Very High (Emergency)

Table 3. Contention probabilities for different user priorities.

User Priority	Contention Probabilities	
	$CP_{\max}$	$CP_{\min}$
0	1/8	1/16
1	1/4	1/16
2	1/2	1/8
3	1	1/2

T_s and T_D are the durations of the time slot and the interbeacon interval, respectively. N_s and N_{CM} represent the number of available time slots in the SAP and the C/M period, respectively. For the busy channel case, the SmartBAN defines a back-off mechanism for a transmission reattempt. Interframe spaces (IFSs) were provided to separate the data and acknowledgment (ACK) frames.

3. System Model

3.1. Use Case

This research supposes the following use case. The worker wearing the SmartBAN is monitored by an artificial intelligence (AI)-based operator in a factory as shown in Figure 3. The type of sensor node and the target data rate are listed in Table 4. Those target data rates were referred from [28–31]. It was assumed that the hub and the AI-based operator performed bidirectional communication by a wireless communication system with a sufficient channel capacity, such as the fourth generation (4G) and fifth generation (5G) mobile communications systems, Wi-Fi 6 and so on. The AI-based operator monitored vital sign data, video and audio from the worker. The codecs for video and audio were assumed to be H.264 and Advanced Audio Coding (AAC), respectively. Therefore, a discrete cosine transform (DCT) was applied to those data. In addition, the AI-based operator transmitted instruction information to the worker's smart glasses. The relationship between the data rate and the video resolution was as follows: 500 kbps, 700 kbps, 1100 kbps and 2500 kbps corresponding to 426 × 240, 640 × 360, 854 × 480 (standard definition (SD)) and 1280 × 720 (high-definition (HD)), respectively [31].

3.2. Modified PHY

As shown in Table 1, the maximum throughput of the SmartBAN PHY was 1.0 tMbit/sec. Thus, it was not enough to transmit and receive data from all the sensors shown in Table 4. In other words, the data rate of the SmartBAN PHY needed to be improved. Two approaches were considered in this research.

The first approach was applying multilevel PSK modulation to the SmartBAN PHY. Multilevel PSK modulation is available in other types of short-range wireless communication technology, such as $\pi/4$-differential quadrature phase shift keying (DQPSK) and $\pi/8$-differential eight phase shift keying (D8PSK) in the Bluetooth Basic Rate/Enhanced Data Rate (BR/EDR) and IEEE Std. 802.15.6. Hence, these modulation schemes could be applied to the sensors used in the SmartBAN PHY. In this instance, the preamble structure was mentioned when the multilevel PSK was applied. The modified preamble structure was proposed in [32]. The reason for this was that the preamble structure shown in Figure 1 was too simple to perform highly reliable communication dealing with medical and healthcare information. To correctly detect the position of the PLCP header, an start

frame delimiter (SFD) was added between the two-octet preamble and the PLCP header. Cross-correlation was performed on the known modulated SFD symbol when detecting the header position. However, the number of preambles and SFD symbols decreased according to the number of multilevels when multivalued PSK was applied; that is, the header detection capability deteriorated, since the cross-correlation value decreased. Therefore, this problem was addressed by repeating the preamble and the SFD according to the number of multilevels. Figure 4 shows the case where $\log_2 M = 2$. In this equation, M denotes the number of multilevels.

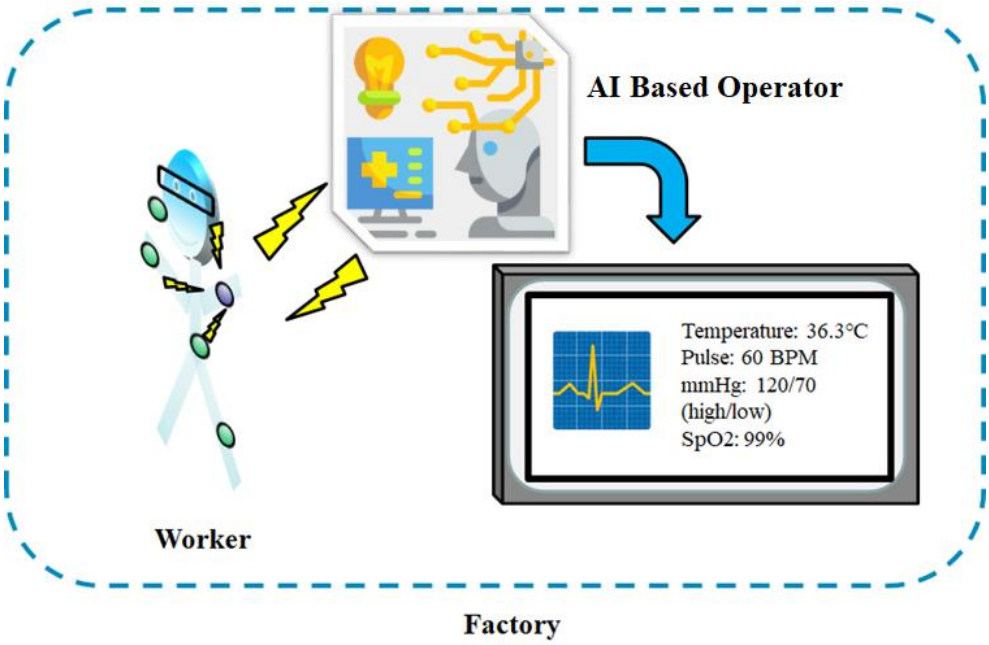

Figure 3. Supposed use case. The artificial intelligence (AI)-based operator monitors the vital data of the worker in the factory wearing the smart body area network (SmartBAN).

Table 4. List of sensors and target data rates.

Sensor Number	Sensor Type	Target Data Rate (R_i)	User Priority
1	SpO2	17.3 kbps	1
2	ECG	24 kbps	1
3	Accelerometer	1.2 kbps	1
4	Pulse rate	8 bps	0
5	Blood pressure	8 bps	0
6	Temperature	8 bps	0
7	Audio (downlink)	128 kbps	2
8	Video (downlink)	700 kbps	2
9	Audio (uplink)	128 kbps	2
10	Video (uplink)	500, 700, 1100 and 2500 kbps	2

The second approach was increasing the symbol rate, with that of SmartBAN being 1.0 Msps as shown in Table 4. On the other hand, each channel bandwidth was 2 MHz. Hence, the symbol rate may have been increased. Figure 5a–c illustrates the normalized power spectral density (PSD) of GFSK and PSK in the constant symbol rate case [33]. As shown in those figures, it was possible to suppress intersymbol interference with adjacent channels by applying a raised cosine filter having a roll-off rate of 0.33 to PSK modulation for the case where the symbol rate was 1.5 Msps. On the other hand, intersymbol interference to adjacent channels due to out-of-band radiation could not be avoided in the case

where the symbol rate was 2.0 Msps. Hence, this case needed to monitor the use status of the adjacent channel.

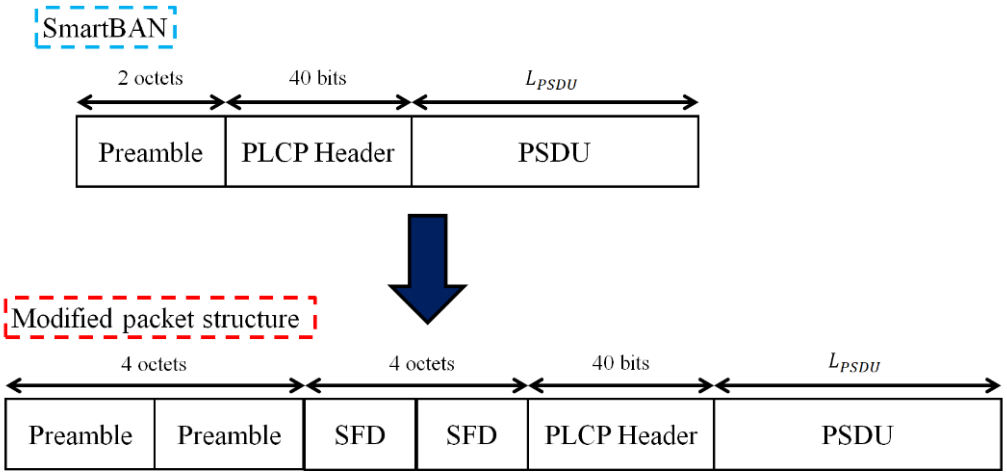

Figure 4. Modified packet structure. The top section of the figure shows the SmartBAN packet structure. The bottom section shows the proposed structure for the case where $\log_2 M = 2$.

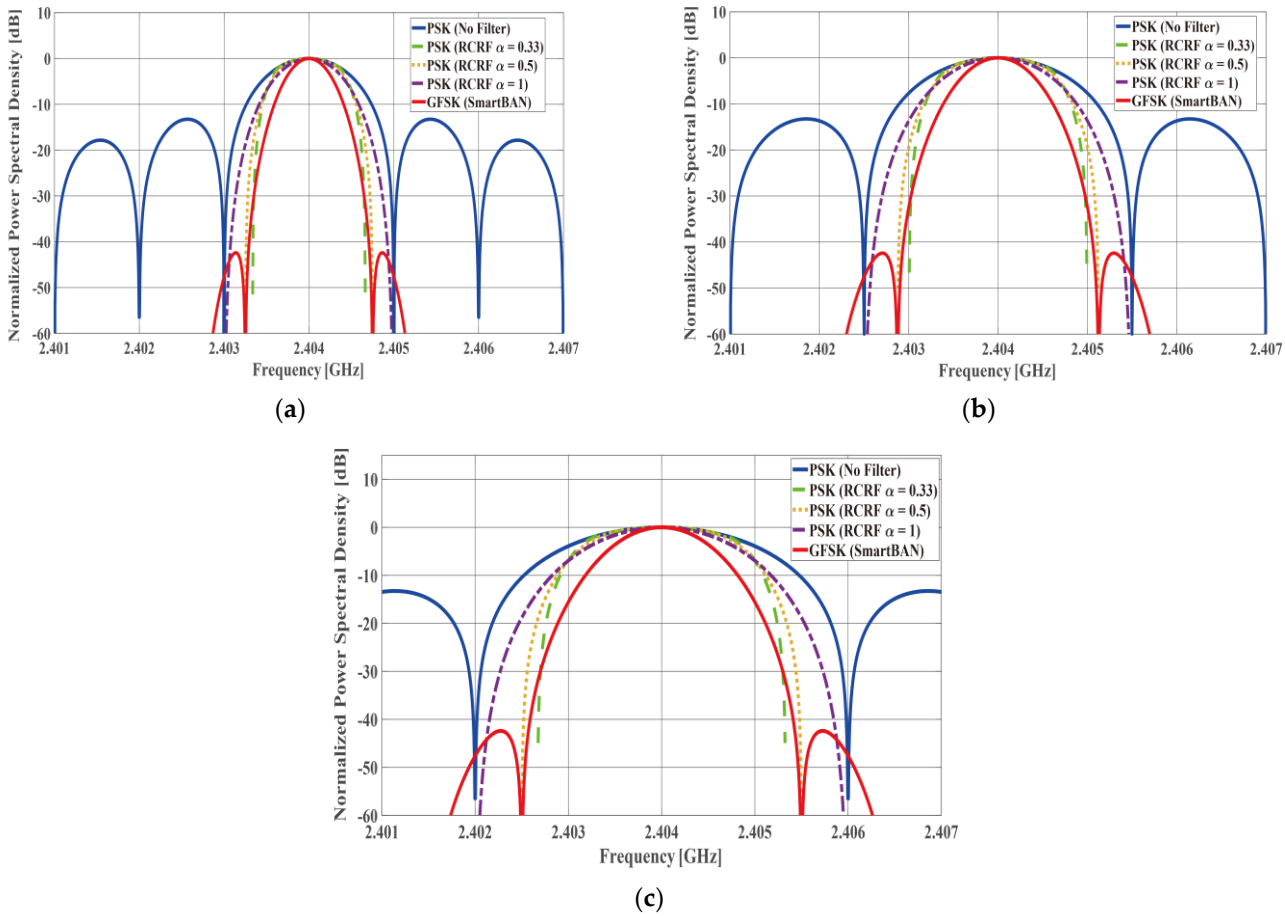

Figure 5. Normalized power spectral density (PSD) of Gaussian frequency shift keying (GFSK) and phase shift keying (PSK) in several constant R_s cases. (**a**) R_s = 1.0 Msps. (**b**) R_s = 1.5 Msps. (**c**) R_s = 2.0 Msps.

3.3. Mathematical Model

The energy efficiency in the PHY layer was derived from [32] as follows:

$$\eta \equiv \frac{P_{succ} L_{info}}{E_{link}} \tag{2}$$

In this equation, L_{info} is the information bit length in the PSDU, E_{link} is the energy consumption of the communication link and P_{succ} is the transmission success ratio. P_{succ} can be expressed as follows [32]:

$$P_{succ} = 1 - PER = \left(1 - P_{fail,preamble}\right)(1 - P_{e,PLCPheader})(1 - P_{e,PSDU}) \tag{3}$$

In this equation, PER is the packet error ratio, $P_{e,preamble}$ is the PLCP header detection failure ratio, $P_{e,PLCPheader}$ is the PLCP header error ratio and $P_{e,PSDU}$ is the PSDU error ratio. Additionally, E_{link} can be simply described as follows [32]:

$$E_{link} = L_{PPDU}(P_{tx} + P_{rx})/R_s + (\varepsilon_{enc} + \varepsilon_{dec}) \tag{4}$$

$$L_{PPDU} = L_{preamble} + L_{SFD} + L_{PLCPheader} + L_{PSDU} \tag{5}$$

In this equation, L_{PPDU}, $L_{preamble}$, L_{SFD}, $L_{PLCPheader}$ and L_{PSDU} are the lengths of the PPDU, the preamble, the SFD, the PLCP header and the PSDU, respectively; P_{tx} and P_{rx} are the transmitter and receiver power consumption, respectively; and ε_{enc} and ε_{dec} are the encoding and decoding energies, respectively.

As a channel model, this research assumed the additive white Gaussian noise (AWGN) channel and IEEE model CM3, which is a channel model of a wearable WBAN [32]. Similarly, the IEEE model CM3 was applied to the path loss model. The path loss model of IEEE model CM3 when using the 2.4 GHz band is as follows [34]:

$$PL(d) = a \times log_{10} d + b + N \tag{6}$$

In this equation, a and b are the coefficients of linear fitting, d is the Tx-Rx distance in mm and N is a normally distributed variable with a standard deviation σ_N. The K factor in decibels (K_{dB}) and each parameter when assuming frequency-flat fading are as shown in Equation (7) [34]:

$$K_{dB} = K_0 - m_k PL(d) + \sigma_k n_k \tag{7}$$

The meaning of each parameter was defined in [34]. K_0 is the fit with the measurement data for the K factor for low path loss, m_k is the slope of the linear correlation between the path loss and the K factor, σ_k is the log-normal variance of the measured data between the path loss and the K factor and n_k is the zero mean and unit variance Gaussian random variable.

Next, the interbeacon interval T_D is described as follows [14–16,27]:

$$T_D = T_{SAP} + T_{CM} + T_{IP} \tag{8}$$

$$T_{SAP} = N_s T_s \tag{9}$$

$$N_s = \sum_{i=1}^{N_{node}} N_{s,i} \tag{10}$$

$$T_{CM} = N_{CM} T_s \tag{11}$$

In this equation, T_{sAP}, T_{CM} and T_{IP} are the durations of the SAP, the C/M period and the inactive period, respectively. Then, $N_{s,i}$ represents the number of available time slots

for each node in the SAP. N_{node} is also the number of nodes in the network. In addition, the number of available time slots, except the inactive period N_D, is calculated as follows:

$$N_D = \left\lfloor \frac{T_D - T_{IP}}{T_s} \right\rfloor \tag{12}$$

$$T_s = \frac{L_{PPDU} + L_{PPDU,ACK}}{R_b} + 2T_{IFS} \tag{13}$$

In this equation, L_{PPDU} and $L_{PPDU,ACK}$ are the PPDU lengths of the data and ACK frames, respectively. T_{IFS} is the duration of the interframe spaces. R_b is also the bit rate. Let r_{sAP}:r_{CM} be the preset ratio of N_s and N_{CM}. N_s and N_{CM} are calculated as follows:

$$N_{CM} = \left\lfloor \frac{r_{CM} N_D}{r_{sAP} + r_{CM}} \right\rfloor \tag{14}$$

$$N_s = N_D - N_{CM} \tag{15}$$

Next, the required $N_{s,i}$ ($\hat{N_{s,i}}$) is calculated as follows:

$$\hat{N_{s,i}} = \left\lceil \frac{R_i T_s}{L_{PSDU}} \right\rceil \tag{16}$$

However, it is assumed that $N_{s,i}$ cannot be fully allocated according to R_i and T_s. Therefore, $N_{s,i}$ is determined using the following criterion. First, in the case where $i \neq N_{node}$, $N_{s,i}$ is assigned as in Equation (16) when $N_s \geq \sum_{i=1}^{N_{node}} \hat{N_{s,i}}$. Second, $N_{s,N_{node}}$ is assigned in the case as follows:

$$N_{s,N_{node}} = N_s - \sum_{i=1}^{N_{node}-1} N_{s,i} \left(N_s \geq \sum_{i=1}^{N_{node}} \hat{N_{s,i}} \right) \tag{17}$$

On the other hand, $N_{s,i}$ is assigned as follows when $N_s < \sum_{i=1}^{N_{node}} \hat{N_{s,i}}$:

$$N_{s,i} = \begin{cases} \hat{N_{s,i}} (i < l) \\ N_s - \sum_{i=1}^{l-1} N_{s,i} (i = l) \\ 0 \ (i > l) \end{cases} \tag{18}$$

where l denotes the limited number of nodes assigned time slots in the SAP. Nodes not assigned time slots in the SAP can transmit data frames in the C/M period.

4. Results and Discussion

4.1. PHY Performance

4.1.1. Computer Simulation Parameters

This subsection describes the performance evaluation by computer simulations of the PLCP header detection, packet error ratio and energy efficiency in the SmartBAN PHY. Since this research did not consider the performance between the operator and the hub, the performance of the body area network was the only focus. The main parameters of the computer simulations are listed in Table 5. The computer simulator was constructed by MATLAB. Then, the comm. PreambleDetector system object in MATLAB was used for preamble detection, and the detection threshold was set to the length of each SFD minus one ($L_{SFD} - 1$). The entire two-octet preamble was only correlated for the SmartBAN, and the threshold was set to the length of the preamble minus one ($L_{preamble} - 1$). Table 6 summarizes the SFDs used in the computer simulations. The reason for choosing these sequences was that they could be handled in units of octets. Table 7 also lists the parameters of the IEEE model CM3 in the hospital room case.

Table 5. Computer simulation parameters.

Parameter	Detail
Channel model	AWGN, IEEE model CM3
Path loss model	IEEE model CM3 (Hospital Room)
Frequency spectrum	2401–2481 MHz
Bandwidth (BW)	2 MHz
Modulation	GFSK, QPSK, $\pi/4$-DQPSK, D8PSK
Bandwidth-time product (BT)	0.5
Modulation index (h)	0.5
ECC (PLCP Header)	(36, 22) shortened BCH code
ECC (PSDU)	(127, 113) BCH code, (127, 85) BCH code
Maximum transmission power (P_{tr})	4 dBm
Thermal noise density (N_0)	−174 dBm/Hz
Implementation losses (I_{dB})	6 dB
Receiver noise figure (NF_{dB})	13 dB
PSDU length (L_{PSDU})	127 bytes
ACK PSDU length ($L_{PSDU,ACK}$)	127 bits
Preamble length ($L_{preamble}$)	2 octets
PLCP header length ($L_{PLCPheader}$)	40 bits
Symbol rate (R_S)	1.0 Msps
Interframe spacing duration (T_{IFS})	150 µs

Table 6. SFD used in computer simulations.

Sequence Type	Bit Sequence (Hexadecimal)
TI CC2650 sync word [35,36]	1101001110010001 (0xD391)
ITU-T Rec. H223 16-bit flag [37]	1000011110110010 (0x87B2)
Orthogonal M-sequence [38]	1111010110010000 (0xF590)
Manchester- coded Orthogonal M-sequence [38]	1010100101100101 (0xA965)

Table 7. Parameters of the IEEE model CM3.

Parameter	Detail
a	6.6
b	36.1
σ_N	3.8
K_0 [dB]	30.6
m_k [dB]	0.43
σ_k	3.4

4.1.2. PLCP Header Detection Failure Ratio

Figures 6–8 show the PLCP header detection failure ratio in the case of several modulation schemes under the AWGN channel, the IEEE model CM3 in the medium shadowing case and the IEEE model CM3 in the strong shadowing case, respectively, as a function of the energy per symbol to noise power spectral density (E_s/N_0). Equations (6) and (7) included a Gaussian random variable representing the effect of shadowing. In other words, the medium shadowing case meant that $N = n_k = 0$, while $N = 3\sigma_N$, $n_k = -3$ in the strong shadowing case. In the medium shadowing case, the K factor's true value was calculated as 4.5 when $d \cong 1.0$ m from (6) and (7). Similarly, that of the strong shadowing case was derived as 0.14 when $d \cong 1.0$ m. In all modulation schemes, the proposed scheme using the SFD suppressed the detection failure ratio, rather than only the SmartBAN preamble. The reason for this was that the cross-correlation value of the sequences used in the SFDs was superior to that of the SmartBAN preamble. Regarding the proposed scheme using the SFD, there was almost no difference in performance, depending on the sequences. In addition, performances less than 10^{-4} were obtained by improving the E_s/N_0 value. On the other hand, the performance of the detection failure rate converged

for GFSK modulation. Even with the proposed scheme, it did not achieve 10^{-3}. Then, the detection failure ratio was slightly improved by increasing the number of modulation levels. This occurred because the improvement of the cross-correlation value by repeating the preamble and the SFD according to the number of modulation levels had an effect.

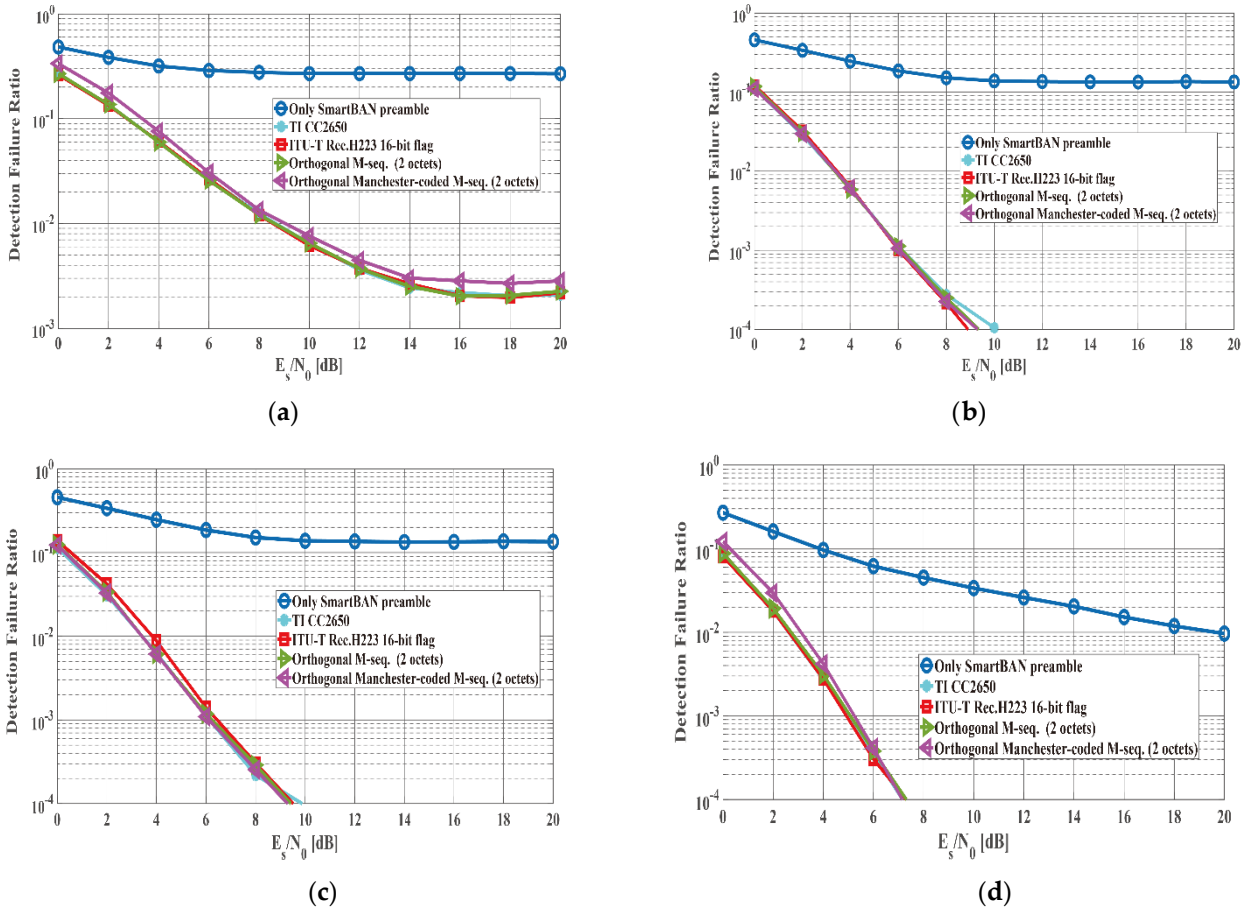

Figure 6. Physical layer convergence protocol (PLCP) header detection failure ratio in the case of several modulation schemes under the additive white Gaussian noise (AWGN) channel. (**a**) GFSK (SmartBAN) (**b**) QPSK (quadrature phase shift keying). (**c**) $\pi/4$-DQPSK (differential quadrature phase shift keying). (**d**) D8PSK.

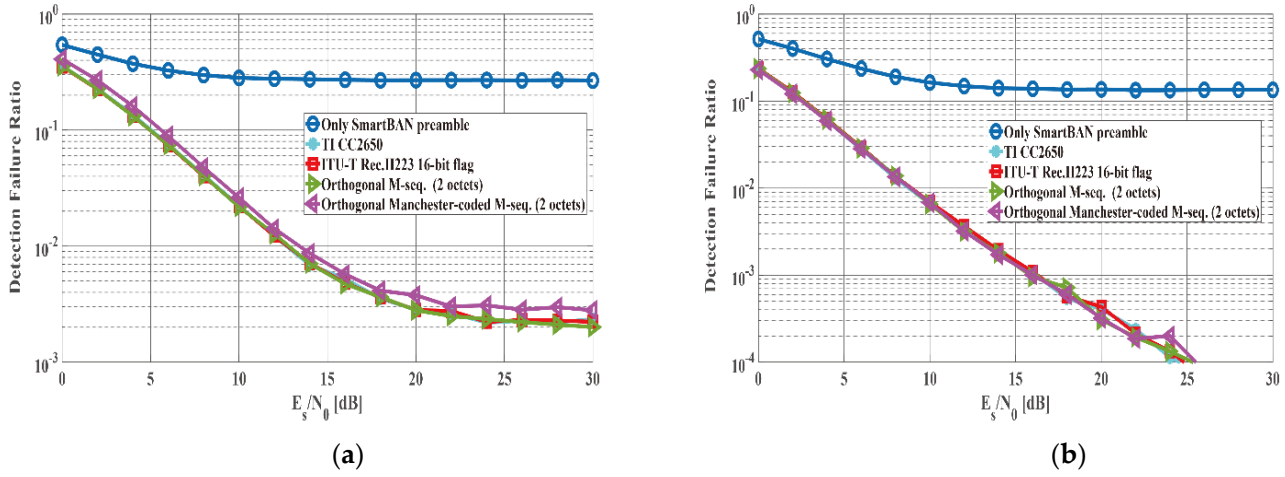

Figure 7. *Cont.*

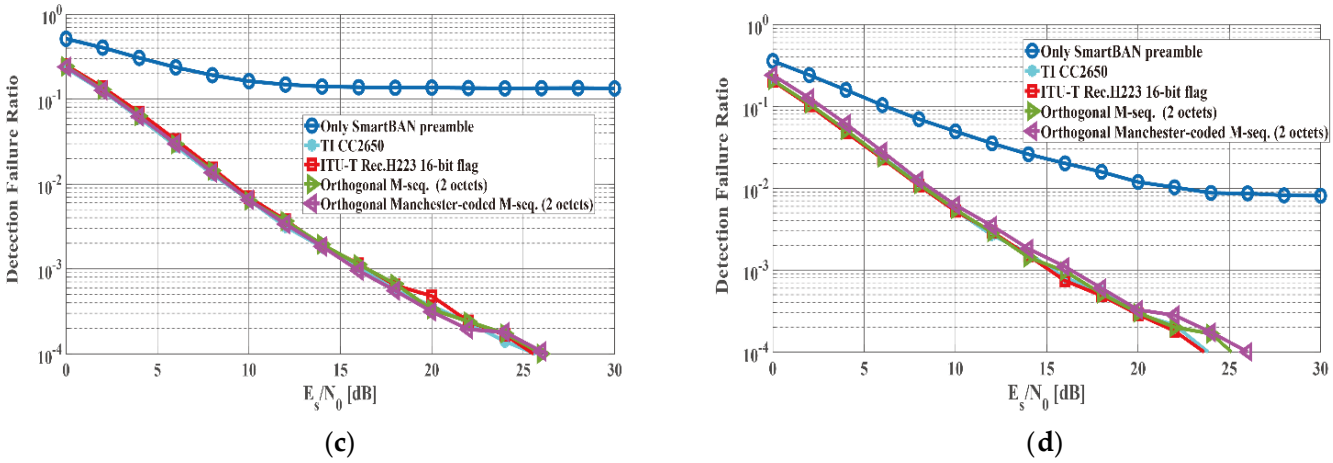

Figure 7. PLCP header detection failure ratio in the case of several modulation schemes under the IEEE channel CM3 (medium shadowing case, $K = 4.5$). (**a**) GFSK (SmartBAN). (**b**) QPSK. (**c**) $\pi/4$-DQPSK. (**d**) D8PSK.

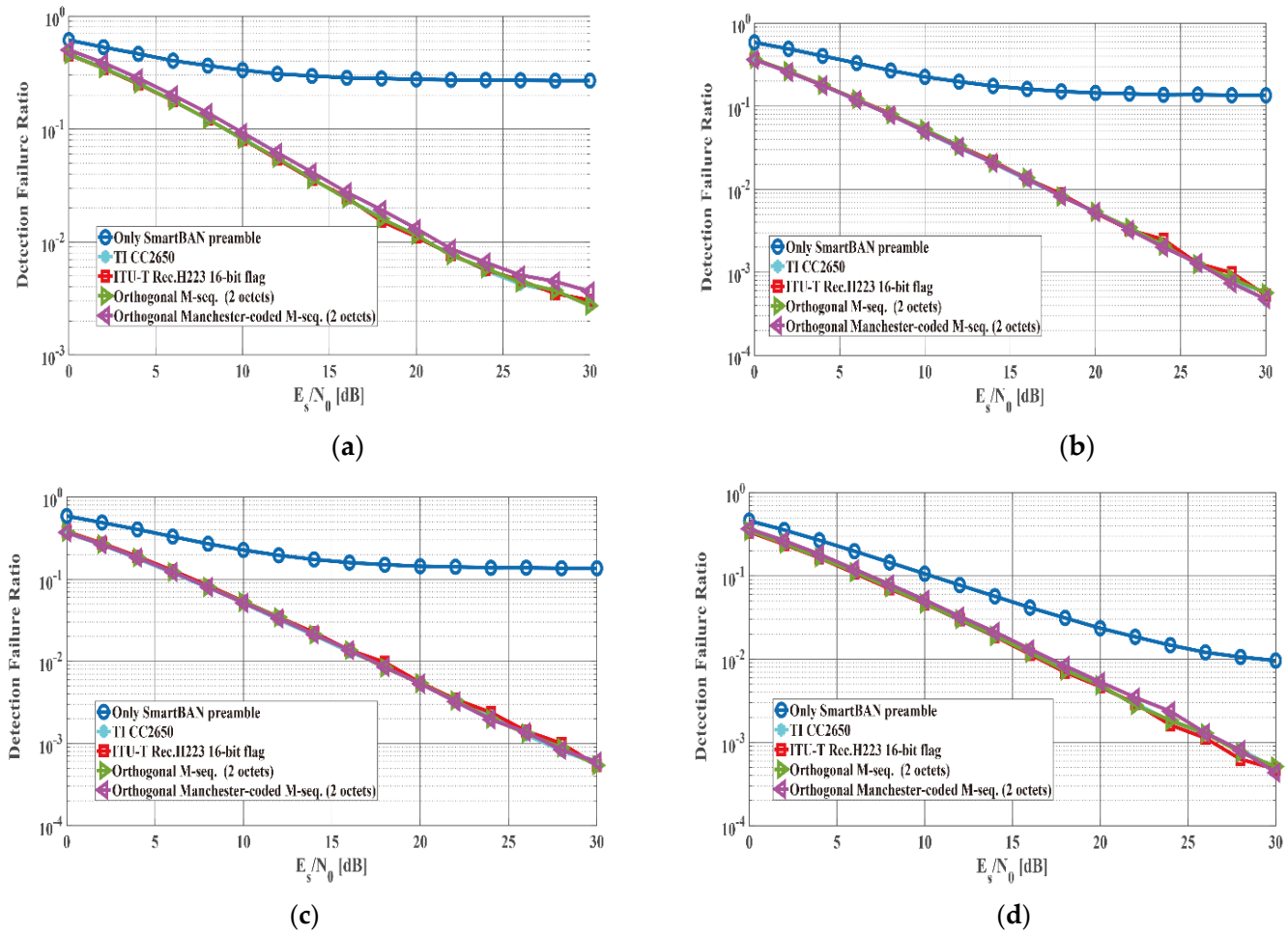

Figure 8. PLCP header detection failure ratio in the case of several modulation schemes under the IEEE channel CM3 (strong shadowing case, $K = 0.14$). (**a**) GFSK (SmartBAN). (**b**) QPSK. (**c**) $\pi/4$-DQPSK. (**d**) D8PSK.

4.1.3. Packet Error Ratio and Energy Efficiency

Figures 9 and 10 show the packet error ratio (PER) and the energy efficiency in the case of several modulation schemes under the AWGN channel, the IEEE model CM3 in the medium shadowing case and the IEEE model CM3 in the strong shadowing case,

respectively, as a function of E_s/N_0. Tables 8 and 9 also summarize E_s/N_0, satisfying PER $\leq 10^{-2}$ and 10^{-3}, respectively. In this instance, the PER included not only bit errors in the PLCP header and the PSDU but also failures in PLCP header detection. Additionally, the proposed scheme utilizing the SFD for detection of the PLCP header was applied, using the TI CC2650 sync word as an SFD. Regarding the PER, the GFSK modulation had the best performance, whereas D8PSK had the best energy efficiency at E_s/N_0, where PER was 10^{-2} or less. Comparing GFSK and QPSK, the unencoded GFSK and (127, 113) BCH-coded QPSK obtained almost the same performance in terms of the PER. However, the energy efficiency of the encoded QPSK was higher than that of GFSK. Comparing QPSK with $\pi/4$-DQPSK, the difference in the PER and the energy efficiency was approximately 3 dB. The difference was not large, since QPSK needed to control the peak-to-average power ratio (PAPR). Comparing $\pi/4$-DQPSK and D8PSK, the unencoded $\pi/4$-DQPSK and (127, 85) BCH-coded D8PSK obtained almost the same PER performance. On the other hand, the energy efficiency of the encoded D8PSK was smaller than that of the unencoded $\pi/4$-DQPSK. Thus, (127, 85) BCH coding was not effective in this performance comparison.

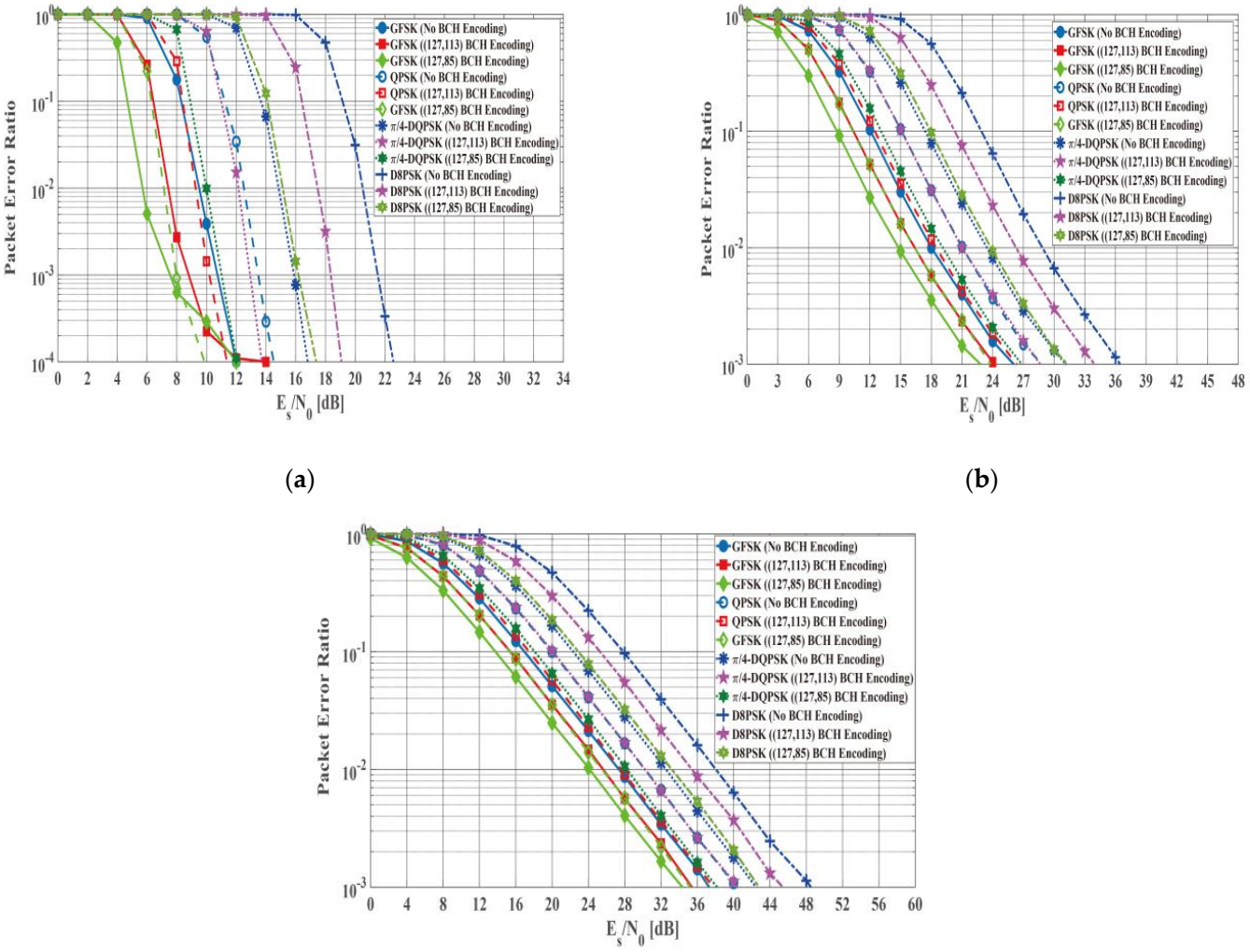

(**a**) (**b**)

(**c**)

Figure 9. Packet error ratio in the case of several channel models. (**a**) AWGN. (**b**) IEEE model CM3 (medium shadowing case, K = 4.5). (**c**) IEEE model CM3 (strong shadowing case, K = 0.14).

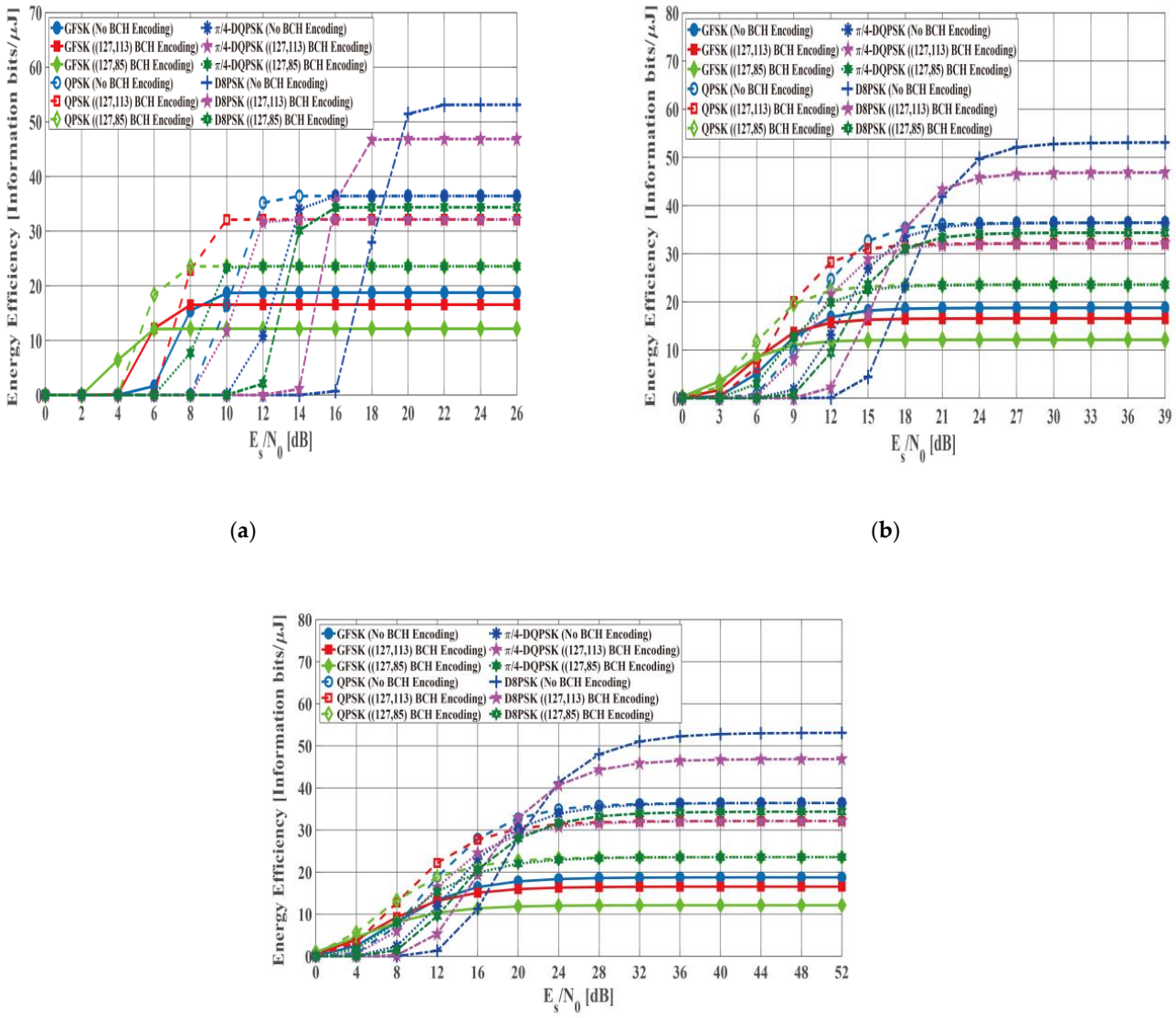

Figure 10. Energy efficiency in the case of several channel models. (**a**) AWGN. (**b**) IEEE model CM3 (medium shadowing case, $K = 4.5$). (**c**) IEEE model CM3 (strong shadowing case, $K = 0.14$).

Table 8. E_s / N_0 (dB) satisfying a packet error ratio (PER) $\leq 10^{-2}$.

Channel Model	ECC	GFSK	QPSK	$\pi/4$ Shift DQPSK	D8PSK
AWGN	No ECC	9.5	12.5	14.8	20.6
	(127, 113) BCH	7.5	9.3	12.1	17.5
	(127, 85) BCH	5.6	7.1	10.0	15.1
CM3 (medium shadowing case)	No ECC	18.0	21.0	23.5	29.8
	(127, 113) BCH	16.5	18.5	21.0	26.2
	(127, 85) BCH	14.8	16.5	19.0	23.8
CM3 (strong shadowing case)	No ECC	24.0	27.2	29.6	38.0
	(127, 113) BCH	22.6	24.8	27.2	35.4
	(127, 85) BCH	21.0	22.5	25.1	33.1

Table 9. E_s/N_0 (dB) satisfying PER $\leq 10^{-3}$.

Channel Model	ECC	GFSK	QPSK	$\pi/4$ Shift DQPSK	D8PSK
AWGN	No ECC	11.8	13.5	16.9	21.6
	(127, 113) BCH	9.8	10.2	12.9	18.3
	(127, 85) BCH	7.6	8.0	11.0	16.2
CM3 (medium shadowing case)	No ECC	26.0	28.5	31.2	36.4
	(127, 113) BCH	24.0	26.2	28.5	34.8
	(127, 85) BCH	22.8	24.0	27.0	31.2
CM3 (strong shadowing case)	No ECC	37.0	40.1	42.6	48.4
	(127, 113) BCH	35.1	37.6	40.1	45.2
	(127, 85) BCH	34.2	35.1	38.0	42.9

4.1.4. Link Budget and Receiver Sensitivity

The link budget is calculated as follows:

$$\begin{gathered} P_{\mathrm{rx}} = P_{\mathrm{tx}} + G_{\mathrm{tx}} - L_{\mathrm{tx}} - L_{\mathrm{path}} + G_{\mathrm{rx}} - L_{\mathrm{rx}} \\ L_{\mathrm{path}} = L_{\mathrm{fs}} + L_{\mathrm{m}} \end{gathered} \tag{19}$$

In this equation, P_{rx} and P_{tx} are the receiver and transmitter power, respectively, G_{tx} and G_{rx} are the antenna gain at the transmitter and receiver, respectively, and L_{tx} and are the transmitter and receiver losses, respectively. L_{path} is a path loss, L_{fs} is a free space loss, and L_{m} is miscellaneous losses, such as fading loss and body loss. When P_{tx} = 4 dBm, G_{tx} and G_{rx} = 3 dBi, L_{tx} and L_{rx} = 3 dB and L_{path} = 53.9 dB (calculated by Equation (6)), the calculation example of the link budget is as follows:

$$P_{\mathrm{rx}} = 4 + 3 - 3 - 53.9 + 3 - 3 = -49.9 \text{ dBm} \tag{20}$$

Then, the receiver sensitivity (S_{dBm}) and the fade margin are also calculated as follows:

$$S_{\mathrm{dBm}} = -174 \text{ (dBm)} + NF_{\mathrm{dB}} + E_b/N_0 \text{ (dB)} + 10 \log_{10} R_s + I_{\mathrm{dB}} \tag{21}$$

$$E_b/N_0 = E_s/N_0 \times R_c/\log_2 M \tag{22}$$

$$\text{Fade margin} = P_{\mathrm{rx}} - S_{\mathrm{dBm}} \tag{23}$$

In this equation, NF_{dB} is a noise value, R_c is a coding rate and I_{dB} is an implemental loss. Tables 10 and 11 summarize examples of S_{dBm} under the AWGN channel in the case of PER $\leq 10^{-2}$ and 10^{-3}, respectively. Tables 12 and 13 also summarize examples of fade margins in cases where PER $\leq 10^{-2}$ and 10^{-3}, respectively. As shown in Tables 8 and 9 again, the differences in E_s/N_0 satisfying PER $\leq 10^{-2}$ and 10^{-3} between the AWGN channel and the IEEE model CM3 in the medium shadowing case were approximately 8.5 dB and 15 dB, respectively. Hence, it can be said that the fade margin was sufficiently obtained from those tables without using an ECC. On the other hand, those between the AWGN channel and the IEEE model CM3 in the strong shadowing case were approximately 15 dB and 26 dB, respectively. Comparing them with Tables 12 and 13, the sufficient fade margin could be obtained in a case where PER $\leq 10^{-2}$, while it was also found that the uncoded $\pi/4$-DQPSK and D8PSK did not provide a sufficient fade margin in a case where PER $\leq 10^{-3}$. However, it can be said that those modulation schemes were also sufficiently useful, because the energy efficiency was sufficiently large even in cases where PER $\leq 10^{-2}$.

Table 10. Examples of S_{dBm} (dBm). PER $\leq 10^{-2}$, L_{PSDU} = 127 bytes, NF_{dB} = 13 dB and I_{dB} = 6 dB.

ECC	R_s	GFSK	QPSK	π/4 Shift DQPSK	D8PSK
No ECC	1.0	−84.5	−82.0	−79.7	−74.1
	1.5	−82.7	−80.2	−77.9	−72.3
	2.0	−81.5	−79.0	−76.7	−71.0
(127, 113) BCH	1.0	−86.6	−85.3	−82.5	−77.2
	1.5	-84.8	−83.5	−80.7	−75.4
	2.0	−84.6	−82.2	−79.4	−74.2
(127, 85) BCH	1.0	−88.7	−87.6	−84.7	−79.7
	1.5	−87.0	−85.8	−82.9	−77.9
	2.0	−85.7	−84.6	−81.7	−76.7

Table 11. Examples of S_{dBm} (dBm). PER $\leq 10^{-3}$, L_{PSDU} = 127 bytes, NF_{dB} = 13 dB and I_{dB} = 6 dB.

ECC	R_s	GFSK	QPSK	π/4 Shift DQPSK	D8PSK
No ECC	1.0	−82.2	−81.0	−77.6	−73.1
	1.5	−80.4	−79.2	−75.8	−71.3
	2.0	−79.2	−78.0	−74.6	−70.1
(127, 113) BCH	1.0	−84.3	−84.4	−81.7	−76.4
	1.5	−82.5	−82.6	−79.9	−74.6
	2.0	−81.3	−81.3	−78.6	−73.4
(127, 85) BCH	1.0	−86.7	−86.7	−83.7	−78.6
	1.5	−85.0	−84.9	−81.9	−76.8
	2.0	−83.7	−83.7	−80.7	−75.6

Table 12. Examples of fade margins (dBm). PER $\leq 10^{-2}$, L_{PSDU} = 127 bytes, NF_{dB} = 13 dB and I_{dB} = 6 dB.

ECC	R_s	GFSK	QPSK	π/4 Shift DQPSK	D8PSK
No ECC	1.0	34.6	32.1	29.8	24.2
	1.5	32.8	30.3	28.0	22.4
	2.0	31.6	29.1	26.8	21.2
(127, 113) BCH	1.0	36.7	35.4	32.6	27.3
	1.5	34.9	33.6	30.8	25.5
	2.0	33.7	32.3	29.5	24.3
(127, 85) BCH	1.0	37.1	35.9	33.0	28.0
	1.5	35.8	34.7	31.8	26.8
	2.0	36.8	36.8	33.8	28.7

Table 13. Examples of fade margins (dBm). PER $\leq 10^{-3}$, L_{PSDU} = 127 bytes, NF_{dB} = 13 dB and I_{dB} = 6 dB.

ECC	R_s	GFSK	QPSK	π/4 Shift DQPSK	D8PSK
No ECC	1.0	32.3	31.1	27.7	23.2
	1.5	30.5	29.3	25.9	21.4
	2.0	29.3	28.1	24.7	20.2
(127, 113) BCH	1.0	34.4	34.5	31.8	26.5
	1.5	32.6	32.7	30.0	24.7
	2.0	31.4	31.4	28.7	23.5
(127, 85) BCH	1.0	36.8	36.8	33.8	28.7
	1.5	35.1	35.0	32.0	26.9
	2.0	33.8	33.8	30.8	25.7

4.2. Network Performance

This subsection describes performance evaluations in the network, such as the average throughput and latency of each sensor node (Tp_i, L_i), as shown in Table 4. In this instance, T_D was set to 250 ms, and $r_{sAP} : r_{CM}$ was set to 9:1. The parameters of the PHY were based on Table 5. In addition, T_{IP} was assumed to be sufficiently shorter than T_D. Tables 14 and 15 list examples of Tp_i and L_i. For the low data rate sensors (sensors 1–6), Tp_i and L_i were not significantly changed regardless of $R_b = R_s \times \log_2 M$ and R_{10}. In particular, L_i was basically within T_D. In other words, those sensors were reliably able to transmit data frames in the interbeacon interval. On the other hand, a lower R_b decreased Tp_i and increased L_i significantly for the high data rate sensors (sensors 7–10). In particular, sensors 8–10 could not transmit enough data at the R_b of the conventional SmartBAN PHY. However, sufficient Tp_i and L_i values were obtained for sensors 7–9, even though R_{10} was changed due to the improvement in the number of modulation levels and R_s. For sensor 10, sufficient Tp_i and L_i values were achieved even when R_{10} = 2500 kbps by setting R_b to 6 Mbps. From the above results, it is necessary to increase the number of modulation levels and the symbol rate to improve the PHY/MAC layer throughput to perform audio or video transmission, as well as the vital sign sensor in the SmartBAN.

Table 14. Examples of Tp_i (kbps).

$R_s \times \log_2 M$ (Mbps)	Target R_{10} (kbps)	Tp_1	Tp_2	Tp_3	Tp_4	Tp_5	Tp_6	Tp_7	Tp_8	Tp_9	Tp_{10}
1.0	500	16.95	23.78	1.117	0.004421	0.005684	0.008526	126.5	522.1	4.916	4.840
	700	16.98	23.80	1.108	0.005052	0.008526	0.004421	126.1	522.1	4.924	4.870
	1100	17.08	23.61	1.154	0.008210	0.01390	0.01137	126.4	521.9	4.929	4.981
	2500	17.12	23.82	1.133	0.01010	0.008526	0.009473	126.3	522.0	4.879	4.931
1.5	500	16.41	23.25	1.039	0.007579	0.008526	0.006631	125.0	697.0	125.7	45.01
	700	16.58	23.13	1.002	0.005210	0.006158	0.006158	125.3	697.0	124.8	45.09
	1100	16.52	23.37	1.032	0.009947	0.008052	0.008526	124.9	697.2	125.6	45.17
	2500	16.72	23.25	1.018	0.006631	0.005684	0.006631	124.8	697.3	125.7	44.93
2.0	500	15.93	22.57	0.8631	0.01053	0.007368	0.003684	123.6	695.8	123.9	405.3
	700	16.01	22.60	0.9221	0.006842	0.01053	0.007368	123.3	695.8	123.7	405.4
	1100	16.00	22.65	0.9442	0.007368	0.009473	0.006842	123.8	695.3	123.6	405.4
	2500	15.91	22.56	0.8568	0.004210	0.009473	0.005789	123.4	695.2	123.7	405.5
3.0	500	14.87	21.50	0.7528	0.003760	0.009776	0.007520	121.2	693.3	121.8	493.9
	700	14.88	21.19	0.7565	0.008272	0.01203	0.007520	121.8	693.6	121.5	694.8
	1100	14.74	21.61	0.7911	0.005264	0.005264	0.006016	121.1	693.9	121.4	1020
	2500	15.01	21.46	0.7550	0.004512	0.006768	0.009776	121.2	694.3	121.6	1020
4.0	500	14.17	20.45	0.6759	0.008460	0.008460	0.005640	119.1	691.4	119.8	492.9
	700	13.80	20.48	0.7191	0.005640	0.006580	0.006580	119.8	691.0	119.0	691.8
	1100	13.90	20.53	0.6627	0.009400	0.003760	0.005640	119.4	691.4	119.2	1092
	2500	13.63	20.47	0.6834	0.006580	0.005640	0.003760	119.5	691.8	118.7	1704
4.5	500	13.72	20.50	0.6775	0.004039	0.009087	0.003029	119.0	690.7	118.9	491.2
	700	13.54	19.94	0.6351	0.004039	0.005049	0.003029	118.6	690.6	118.7	691
	1100	13.77	20.15	0.6876	0.008078	0.004039	0.003029	119.1	691.1	119.3	1092
	2500	13.71	20.22	0.7088	0.009087	0.003029	0.003029	118.5	691.1	118.1	1905
6.0	500	12.82	18.84	0.6738	0.004308	0.002585	0.005170	116.1	688.1	116.1	489.9
	700	12.74	18.63	0.6678	0.006893	0.001723	0.005170	116.3	688.6	115.3	689.4
	1100	12.75	18.89	0.6410	0.004308	0.004308	0.004308	115.8	688.0	115.4	1088
	2500	12.65	18.88	0.6281	0.005170	0.006031	0.004308	115.0	688.7	115.6	2488

Table 15. Examples of L_i (ms).

$R_s \times \log_2 M$ (Mbps)	Target R_{10} (kbps)	L_1	L_2	L_3	L_4	L_5	L_6	L_7	L_8	L_9	L_{10}
1.0	500	174.8	273.6	143.1	85.68	120.8	135.3	132.3	302.6 (s)	93.16 (s)	24.74 (s)
	700	172.7	277.2	141.4	145.8	114.0	141.2	130.1	303.0 (s)	93.13 (s)	17.85 (s)
	1100	174.2	259.2	140.8	118.5	100.4	128.4	131.7	303.6 (s)	93.28 (s)	16.11 (s)
	2500	176.8	267.8	142.1	118.7	99.65	109.0	133.2	302.9 (s)	92.62 (s)	15.85 (s)
1.5	500	155.2	214.6	133.4	150.4	145.5	95.70	125.0	55.97	114.6	93.13 (s)
	700	157.8	206.3	129.3	165.5	137.9	142.9	124.9	56.08	112.5	68.70 (s)
	1100	157.3	208.1	128.7	129.6	131.4	73.31	123.6	55.69	117.3	44.87 (s)
	2500	156.7	195.3	129.5	145.2	115.9	118.2	124.2	56.42	115.6	41.73 (s)
2.0	500	146.0	177.1	125.3	90.52	123.8	133.7	122.8	74.94	107.0	142.5 (s)
	700	147.1	178.8	122.5	140.7	103.5	84.77	122.4	74.91	106.4	234.6 (s)
	1100	147.6	181.5	126.8	153.6	124.3	152.5	122.8	74.63	106.7	225.6 (s)
	2500	147.4	175.7	120.4	117.4	143.2	108.5	121.5	74.05	107.2	185.5 (s)
3.0	500	132.9	149.4	115.4	106.8	97.99	109.0	117.5	89.41	101.9	43.54
	700	132.8	146.1	115.0	98.25	102.2	133.2	118.2	89.74	102.0	50.77
	1100	134.7	152.2	120.3	118.0	96.82	128.4	118.2	90.55	102.8	42.11 (s)
	2500	132.1	153.4	114.9	88.22	112.2	83.28	118.4	89.81	102.9	167.5 (s)
4.0	500	125.5	132.7	108.1	127.4	105.0	83.76	116.4	96.81	99.41	23.32
	700	123.3	134.2	111.6	85.60	168.5	127.1	116.6	97.74	99.22	26.82
	1100	123.8	136.1	109.2	95.95	145.2	103.9	115.5	97.23	99.49	34.37
	2500	124.9	135.4	110.1	92.75	125.5	162.4	116.4	97.44	100.3	116.6 (s)
4.5	500	123.9	132.7	106.6	114.5	115.7	76.54	115.9	97.90	98.58	19.98
	700	123.5	130.9	109.5	101.5	105.2	56.13	115.5	98.58	98.95	22.90
	1100	125.1	131.4	106.9	95.46	151.1	93.79	116.2	99.04	99.49	29.26
	2500	122.6	130.6	108.5	152.1	134.4	109.4	115.5	99.30	98.99	90.24 (s)
6.0	500	118.3	122.7	108.7	138.3	109.5	89.67	114.5	102.9	96.35	10.64
	700	117.6	120.8	107.9	112.3	105.9	83.57	114.9	103.3	97.06	12.37
	1100	118.6	121.5	103.5	120.4	83.51	66.77	114.8	103.7	97.84	15.53
	2500	117.6	123.3	107.0	113.5	118.1	114.0	114.7	104.0	98.21	31.03

5. Conclusions

This research examined the feasibility of a human monitoring system using a SmartBAN which included multimedia devices. Multilevel PSK modulation was applied to the SmartBAN PHY, and the symbol rate was improved by setting the roll-off rate appropriately to realize the system. The numerical results showed that a sufficient link budget, receiver sensitivity and fade margin were obtained even when multilevel PSK modulation and symbol rate improvements were applied to the SmartBAN PHY. It was clear that those techniques were required for audio and video transmission as well as vital sign data transmission in the SmartBAN.

For future work, the feasibility of applying other modulation and error control schemes will be examined for higher-quality audio and video transmission. In addition, the optimization of the access protocol should be considered in this case.

Author Contributions: Conceptualization, K.T. and H.T.; methodology, K.T. and H.T.; software, K.T.; validation, K.T. and H.T.; formal analysis, K.T.; investigation, K.T.; resources, K.T. and K.S.; data curation, K.T. and H.T.; writing—original draft preparation, K.T.; writing—review and editing, K.T., H.T. and K.S.; visualization, K.T.; supervision, H.T. and K.S.; project administration, K.T.; funding acquisition, K.T. All authors have read and agreed to the published version of the manuscript.

Funding: This research received no external funding.

Acknowledgments: The first author would like to thank members of the Kohno Laboratory, Yokohama National University, Japan for their great inspiration and kindness.

Conflicts of Interest: The authors declare no conflict of interest.

References

1. Gatouillat, A.; Badr, Y.; Massot, B.; Sejdić, E. Internet of Medical Things: A Review of Recent Contributions Dealing with Cyber-Physical Systems in Medicine. *IEEE Internet Things J.* **2018**, *5*, 3810–3822. [CrossRef]
2. Limaye, A.; Adegbija, T. HERMIT: A Benchmark Suite for the Internet of Medical Things. *IEEE Internet Things J.* **2018**, *5*, 4212–4222. [CrossRef]
3. Spinsante, S.; Gambi, E. Remote health monitoring for elderly through interactive television. *Biomed. Eng. Online* **2012**, *11*, 1–18. [CrossRef] [PubMed]
4. Costa, C.R.; Anido-Rifón, L.E.; Fernández-Iglesias, M.J. An Open Architecture to Support Social and Health Services in a Smart TV Environment. *IEEE J. Biomed. Health Inform.* **2017**, *21*, 549–560. [CrossRef]
5. Chen, M.; Gonzalez, S.; Vasilakos, A.V.; Cao, H. VCM Leung, Body Area Networks: A Survey. *Mob. Netw. Appl.* **2010**, *16*, 171–193. [CrossRef]
6. Cavallari, R.; Martelli, F.; Rosini, R.; Buratti, C.; Verdone, R. A Survey on Wireless Body Area Networks: Technologies and Design Challenges. *IEEE Commun. Surv. Tutor.* **2014**, *16*, 1635–1657. [CrossRef]
7. Movassaghi, S.; Abolhasan, M.; Lipman, J.; Smith, D.; Jamalipour, A. Wireless Body Area Networks: A Survey. *IEEE Commun. Surv. Tutor.* **2014**, *16*, 1658–1686. [CrossRef]
8. Hayajneh, T.; Almashaqbeh, G.; Ullah, S.; Vasilakos, A.V. A survey of wireless technologies coexistence in WBAN: Analysis and open research issues. *Wirel. Netw.* **2014**, *20*, 2165–2199. [CrossRef]
9. Fortino, G.; Fatta, G.D.; Pathan, M.; Vasilakos, A.V. Cloud-assisted body area networks: State-of-the-art and future challenges. *Wirel. Netw.* **2014**, *20*, 1925–1938. [CrossRef]
10. Ning, Z.; Dong, P.; Wang, X.; Hu, X.; Guo, L.; Hu, B.; Guo, Y.; Qiu, T.; Kwok, R.Y. Mobile Edge Computing Enabled 5G Health Monitoring for Internet of Medical Things: A Decentralized Game Theoretic Approach. *IEEE J. Sel. Areas Commun.* **2021**, *39*, 463–478. [CrossRef]
11. Cao, T.; Tao, L.; Liu, D.; Wang, Q.; Sun, J. Design and Realization of Blood Oxygen and Heart Rate Sensor Nodes in Wireless Body Area Network. In Proceedings of the 2020 IEEE International Conference on Artificial Intelligence and Computer Applications (ICAICA), Dalian, China, 27–29 June 2020.
12. Blunda, L.L.; Gutiérrez-Madroñal, L.; Wagner, M.F.; Medina-Bulo, I. A Wearable Fall Detection System Based on Body Area Networks. *IEEE Access* **2020**, *8*, 193060–193074. [CrossRef]
13. Mehmood, G.; Khan, M.Z.; Waheed, A.; Zareei, M.; Mohamed, E.M. A Trust-Based Energy-Efficient and Reliable Communication Scheme (Trust-Based ERCS) for Remote Patient Monitoring in Wireless Body Area Networks. *IEEE Access* **2020**, *8*, 131397–131413. [CrossRef]
14. Smart Body Area Network (SmartBAN); Low Complexity Medium Access Control (MAC) for SmartBAN. ETSI TC Smart BAN TS 103 325 V1.1.1. 2015. Available online: http://www.etsi.org/deliver/etsi_ts/103300_103399/103325/01.01.01_60/ts_103325v010101p.pdf (accessed on 9 February 2021).
15. Smart Body Area Network (SmartBAN); Enhanced Ultra-Low Power Physical Layer. ETSI TC Smart BAN TS 103 326 V1.1.1. 2015. Available online: https://www.etsi.org/deliver/etsi_ts/103300_103399/103326/01.01.01_60/ts_103326v010101p.pdf (accessed on 9 February 2021).
16. Hämäläinen, M.; Mucchi, L.; Girod-Genet, M.; Paso, T.; Farserotu, J.; Tanaka, H.; Anzai, D.; Pierucci, L.; Khan, R.; Alam, M.M.; et al. ETSI SmartBAN Architecture: The Global Vision for Smart Body Area Networks. *IEEE Access* **2020**, *8*, 150611–150625. [CrossRef]
17. IEEE Standard for Information Technology—Telecommunications and Information Exchange Between Systems—Local and Metropolitan Area Networks; Specific Requirements: Part 15.6: Wireless Medium Access Control (MAC) and Physical Layer (PHY) Specifications for Wireless Personal Area Networks (WPANs) Used in or 12 around A Body. 2012. Available online: https://ieeexplore.ieee.org/document/6161600 (accessed on 9 February 2021).
18. Tanaka, H.; Hatakeyama, Y.; Komori, T.; Saho, S.; Shiode, N. Evaluation of PWTT Based Blood Pressure Fluctuation using Body Area Network. In Proceedings of the IEEE Engineering in Medicine and Biology Society (EMBC'18), Honolulu, HI, USA, 17–21 July 2018.
19. Urata, Y.; Umetani, A. Introduction to Use Scenes of Biodata and Other Field Data in a Smart City. In Proceedings of the ETSI IoT Week 2018, Sophia Antipolis, France, 22–26 October 2018.
20. Din, I.U.; Almogren, A.; Guizani, M.; Zuair, M. A Decade of Internet of Things: Analysis in the Light of Healthcare Applications. *IEEE Access* **2019**, *7*, 89967–89979. [CrossRef]
21. Ang, K.L.; Seng, J.K.P. Application Specific Internet of Things (ASIoTs): Taxonomy, Applications, Use Case and Future Directions. *IEEE Access* **2019**, *7*, 56577–56590. [CrossRef]
22. Syberfeldt, A.; Danielsson, O.; Gustavsson, P. Augmented Reality Smart Glasses in the Smart Factory: Product Evaluation Guidelines and Review of Available Products. *IEEE Access* **2017**, *5*, 9118–9130. [CrossRef]
23. Mourtzis, D.; Siatras, V.; Angelopoulos, J. Real-Time Remote Maintenance Support Based on Augmented Reality (AR). *Appl. Sci.* **2020**, *10*, 1855. [CrossRef]
24. Mourtzis, D.; Zogopoulos, V.; Vlachou, E. Augmented Reality Application to Support Remote Maintenance as a Service in the Robotics Industry. *Procedia Cirp* **2017**, *63*, 46–51. [CrossRef]

25. Ruppert, T.; Jaskó, S.; Holczinger, T.; Abonyi, J. Enabling Technologies for Operator 4.0: A Survey. *Appl. Sci.* **2018**, *8*, 1650. [CrossRef]
26. Khan, R.; Alam, M.M.; Guizani, M. A Flexible Enhanced Throughput and Reduced Overhead (FETRO) MAC Protocol for ETSI SmartBAN. *IEEE Trans. Mob. Comput.* **2020**. Available online: https://ieeexplore.ieee.org/document/9309094 (accessed on 25 February 2021). [CrossRef]
27. Ramis-Bibiloni, J.; Carrasco-Martorell, L. Energy-Efficient and QoS-Aware Link Adaptation with Resource Allocation for Periodical Monitoring Traffic in SmartBANs. *IEEE Access* **2020**, *8*, 13476–13488. [CrossRef]
28. Stojanov, G.; Kulakov, A. *ICT Innovations 2016 Cognitive Functions and Next Generation ICT Systems*; Springer International Publishing: Cham, Switzerland, 2018.
29. MMA8452Q, 3-axis, 12-bit/8-bit Digital Accelerometer, NXP Semiconductors, Data Sheet: Technical Data, Document Number: MMA8452Q. 2016. Available online: https://www.nxp.com/docs/en/data-sheet/MMA8452Q.pdf (accessed on 24 January 2021).
30. White Paper: The AAC Audio Coding Family for Broadcast and Cable TV. Fraunhofer-Gesellschaft. 2013. Available online: https://www.iis.fraunhofer.de/content/dam/iis/de/doc/ame/wp/FraunhoferIIS_White-Paper_AAC-Broadcast-CableTV.pdf (accessed on 24 January 2021).
31. Choose Live Encoder Settings, Bitrates, and Resolutions. Available online: https://support.google.com/youtube/answer/2853702?hl=en#zippy (accessed on 24 January 2021).
32. Takabayashi, K.; Tanaka, H.; Sakakibara, K. Integrated Performance Evaluation of the Smart Body Area Networks Physical Layer for Future Medical and Healthcare IoT. *Sensors* **2019**, *18*, 30. [CrossRef] [PubMed]
33. Middlestead, R.W. *Digital Communications with Emphasis on Data Modems: Theory, Analysis, Design, Simulation, Testing, and Applications*; Wiley: Hoboken, NJ, USA, 2017.
34. Yazdandoost, K.Y.; Sayrafian-Pour, K. Channel Model for Body Area Network (BAN). IEEE P802.15 Working Group for Wireless Personal Area Networks (WPANs), IEEE P802.15-08-0780-10-0006. 2009. Available online: https://mentor.ieee.org/802.15/file/08/15-08-0780-10-0006-tg6-channel-model.pdf (accessed on 28 September 2018).
35. *CC1101 Low-Power Sub1 GHz RF Transceiver Datasheet*; SWRS061I; Texas Instruments: Dallas, TX, USA, 2020. Available online: https://www.ti.com/lit/ds/symlink/cc1101.pdf (accessed on 27 January 2021).
36. *CC13x0, CC26x0 SimpleLink™ Wireless MCU Technical Reference Manual*; SWCU117I; Texas Instruments: Dallas, TX, USA, 2020. Available online: https://www.ti.com/lit/ug/swcu117i/swcu117i.pdf (accessed on 27 January 2021).
37. International Telecommunication Union. Multiplexing protocol for low bit rate multimedia communication. In *ITU-T Recommendation H.223*; International Telecommunication Union: Geneva, Switzerland, 2001.
38. Habuchi, H. Pseudo-Noise Sequences Based on M-sequence and Its Application for Communications. *IEICE Fundam. Rev.* **2009**, *3*, 32–42. (In Japanese) [CrossRef]